Supplementary Information (SI) for ChemComm.
This journal is © The Royal Society of Chemistry 2026

Supplementary Information for

Pathway-Engineered Co-Assembly of Nanorod–Nanosphere Binary Superlattices

*Di Lei,[a] Hao Wang,[a] Ziyue Zheng,[a] Fangyue Wu,[a] Siyu Wan,[a] Dong Yang,[b] Wei Li,[*a,c] Tongtao Li[*a,c] and Angang Dong[*a,c]*

[a]*State Key Laboratory of Porous Materials for Separation and Conversion, Department of Chemistry, and Shanghai Key Laboratory of Molecular Catalysis and Innovative Materials, Fudan University, Shanghai 200438, China. E-mail: weilichem@fudan.edu.cn; ttli@fudan.edu.cn; agdong@fudan.edu.cn*

[b]*State Key Laboratory of Molecule Engineering of Polymers and Department of Macromolecular Science, Fudan University, Shanghai 200433, China.*

[c]*Southwest Research & Design Institute of the Chemical Industry, Chengdu, China.*

Experimental Section

Materials

Rare earth (RE = Y, Yb, Er, Gd, Nd) chlorate hydrates ($RECl_3$ $6H_2O$, 99.9%), iron(III) chloride hexahydrate ($FeCl_3$ $6H_2O$, 97%), 1-octadecene (ODE, 90%), and oleic acid (OA, 90%) were purchased from Sigma-Aldrich. Ammonium fluoride (NH_4F, >98%) was obtained from Alfa Aesar. Sodium hydroxide (NaOH, AR), potassium hydroxide (KOH, AR), oxalic acid dihydrate (>99.5%), methanol (AR), ethanol (AR), and n-hexane (AR) were purchased from Sinopharm Chemical Reagent Co., Ltd. All chemicals were used as received without further purification.

Synthesis of faceted β-$NaYF_4$:Yb/Er nanocrystals (NCs)

The faceted β-$NaYF_4$:Yb/Er NSs used here were synthesized following a literature method.[1] In a typical synthesis of β-$NaYF_4$:Yb/Er NCs, a rare earth chloride hexahydrate mixture consisting of 1 mmol $RECl_3 \cdot 6H_2O$ (comprising 80% Y, 18% Yb, and 2% Er) was combined with 6 mL of OA and 15 mL of ODE in a 50-mL three-neck flask. After degassing, the flask was then heated to 150 °C under a nitrogen atmosphere to yield a clear, homogeneous solution. Upon cooling to room temperature, the solution was treated with 6 mL of methanol containing NaOH (2.5 mmol) and NH_4F (4 mmol). The resultant mixture was gradually heated to 110 °C to ensure the complete evaporation of methanol, followed by a rapid temperature increase to 300 °C and maintenance at this temperature for 1 hour to facilitate NC formation. Upon cooling to room temperature, ethanol was introduced to precipitate the NCs. The precipitated NCs were subjected to a purification process involving washes with hexane and ethanol, performed at least once to ensure removal of impurities. The purified $NaYF_4$:Yb/Er NCs were re-dispersed in hexane for subsequent self-assembly experiments.

Synthesis of colloidal Fe_3O_4 nanospheres (NSs).

Fe_3O_4 NSs with tunable diameters were synthesized by the thermal decomposition of iron oleate.[2] Briefly, 9 g of iron oleate and 1.2 g of OA were dispersed in 45 mL of ODE, and the mixture was degassed at 120 ℃ under vacuum for 1 h. Then, the solution was

heated to 320 ℃ and kept for 1 h under inert atmosphere. The resulting Fe_3O_4 NSs, with OA as ligands, were dispersed in n-hexane for further use.

Self-assembly of binary nanocrystal superlattices (BNSLs)

In a typical process, a 20 μL of n-hexane solution containing the as-formed NRs and NSs with proper concentration ratios was spread on the diethylene glycol (DEG) surface in a Teflon well.[3] The well was covered with a glass slide to control the evaporation rate. A solid film formed on the DEG surface after the complete evaporation of hexane, which can then be transferred to TEM grids or Si wafers for subsequent characterization. By tuning the size ratio, and total concentration of the constituent nanocrystals, BNSLs with diverse structural symmetries and stoichiometries can be fabricated under analogous interfacial assembly conditions.

Selective Etching of Binary Superlattices

Selective etching was carried out following our previously reported protocol for Fe_3O_4-$NaYF_4$ systems.[4] Briefly, the as-assembled superlattices on carbon-coated TEM grids were subjected to thermal treatment for controlled durations, followed by immersion in dilute aqueous oxalic acid for selective removal of one component. As established in our prior study, the etching selectivity is governed by thermally modulated acid resistance and depends on the chemical composition rather than particle shape. Thus, this strategy is directly applicable to the present rod–sphere superlattices, enabling the selective removal of either Fe_3O_4 or $NaYF_4$ while preserving the lattice registry.

Materials characterization

Transmission electron microscopy (TEM) was carried out on a Hitachi HT 7700 microscope (120 kV). High-resolution TEM (HRTEM), high-angle annular dark-field scanning TEM (HAADF-STEM) images, elemental mapping, small-angle electron diffraction (SAED), and wide-angle electron diffraction (WAED) were conducted on a FEI Tecnai G2 F20 S-Twin microscope at an accelerating voltage of 200 kV. Scanning electron microscopy (SEM) images were acquired on a Zeiss GeminiSEM 500 field-emission microscope operated at 3 kV.

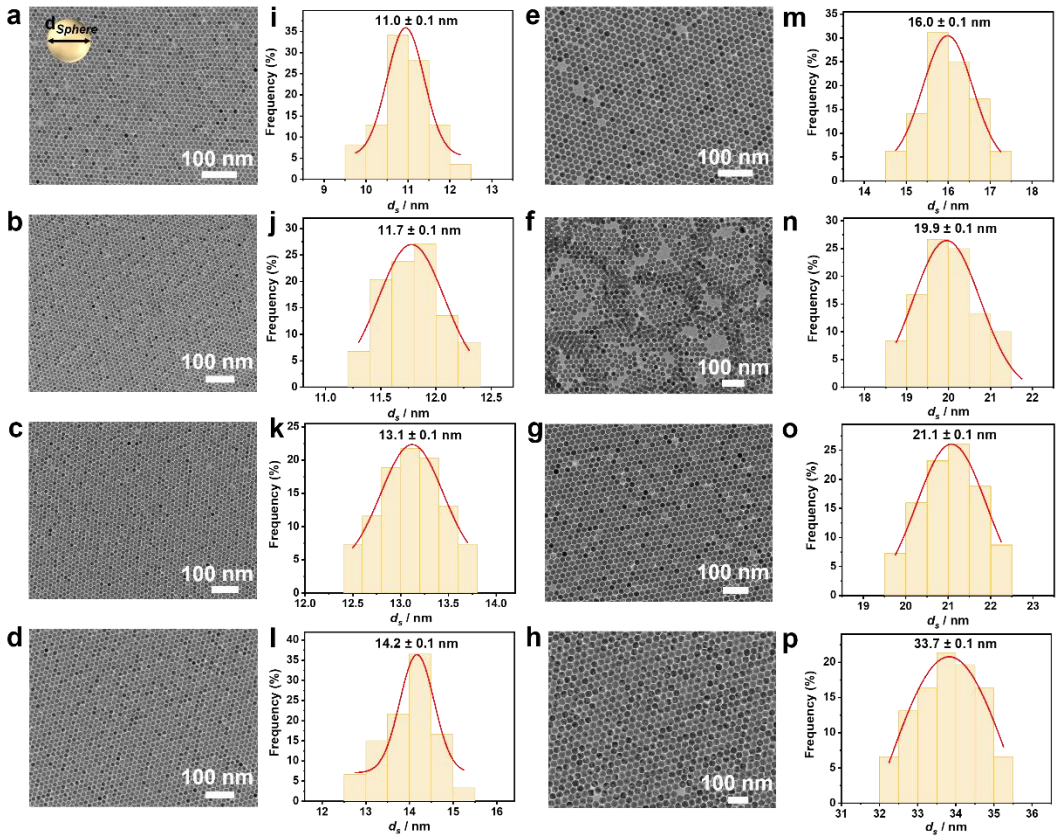

Figure S1. (a–h) TEM images and (i–p) corresponding size distributions of the synthesized nanospheres. (a–g, i–o) Fe_3O_4 NSs with varying diameters: (a, i) 11.0 nm; (b, j) 11.7 nm; (c, k) 13.1 nm; (d, l) 14.2 nm; (e, m) 16.0 nm; (f, n) 19.9 nm; and (g, o) 21.1 nm. (h, p) $NaYF_4$ NSs with an average diameter of 33.7 nm.

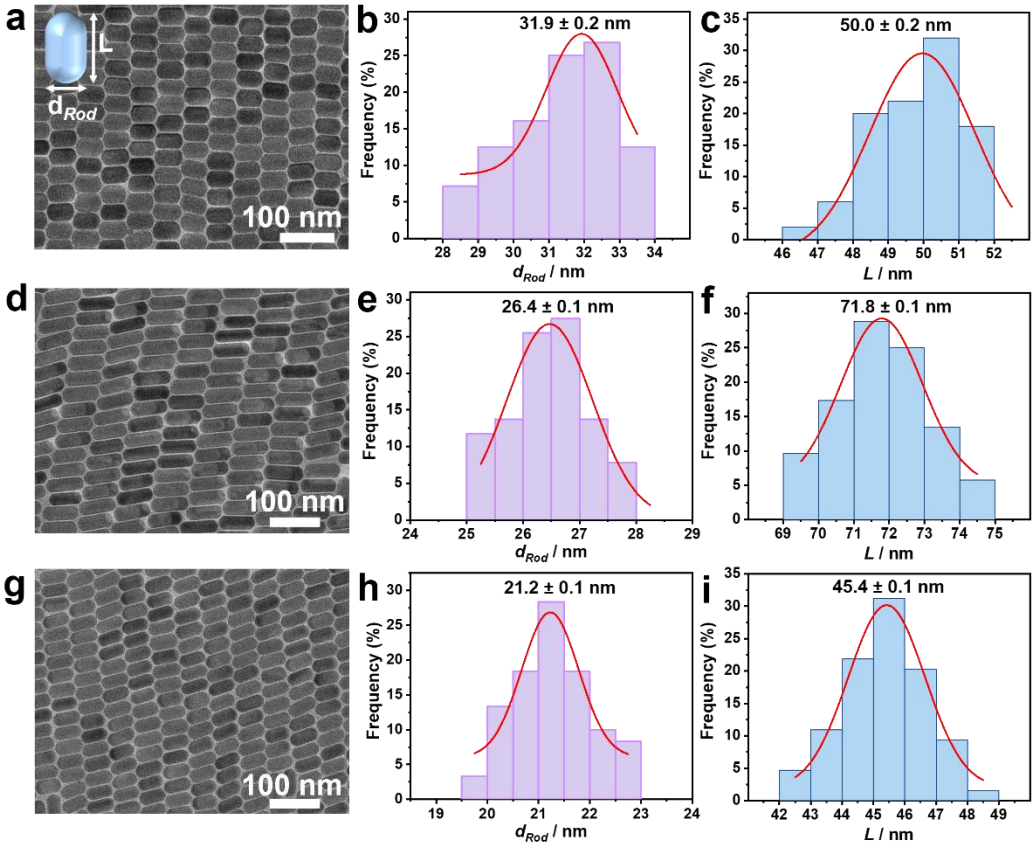

Figure S2. TEM images (left column), histograms of the d_{Rod} distribution (middle column), and histograms of the L distribution (right column) for various nanorods (NRs): (a–c) NR-1; (d–f) NR-2; (g–i) NR-3. d_{Rod} represents the diameter and L represents the length of the nanorods.

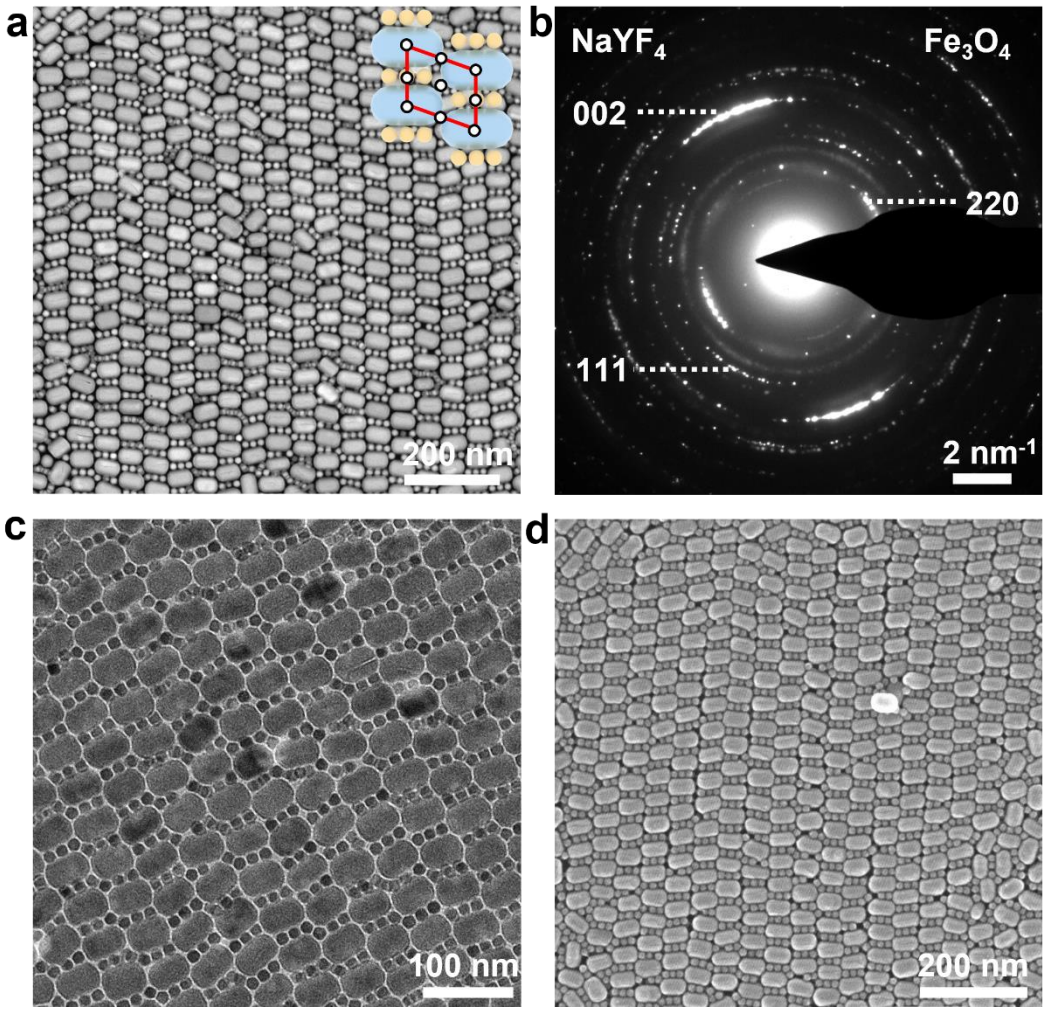

Figure S3. (a) High-magnification HAADF-STEM image of AB_6-*p*2 BNSLs co-assembled from NR-1 and 13.1 nm Fe_3O_4 NSs (inset: schematic of planar wallpaper symmetries with unit cell and symmetry operations); (b) WAED pattern; (c) high-magnification TEM image; (d) SEM image. The result shows that increasing the sphere-to-rod ratio leads to a sphere-rich packing motif, where nanospheres densely fill the interstitial regions of the nanorod array.

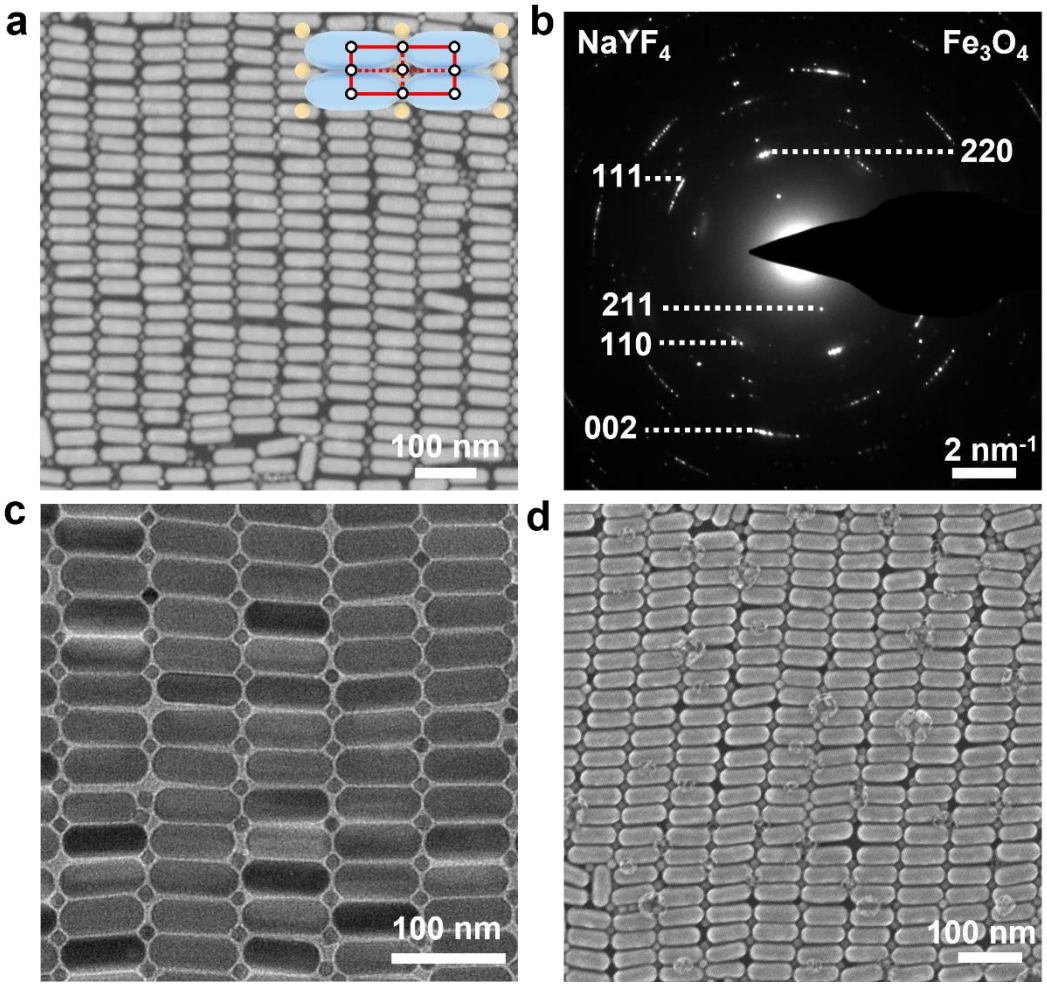

Figure S4. (a) HAADF-STEM image of AB-*pmm* BNSLs co-assembled from NR-2 and 13.1 nm Fe_3O_4 NSs (inset: schematic of planar wallpaper symmetries with unit cell and symmetry operations); (b) WAED pattern; (c) high-magnification TEM image; (d) SEM image. The SEM observation shows a monolayer packing configuration, where NSs occupy the interstitial spaces between the NRs.

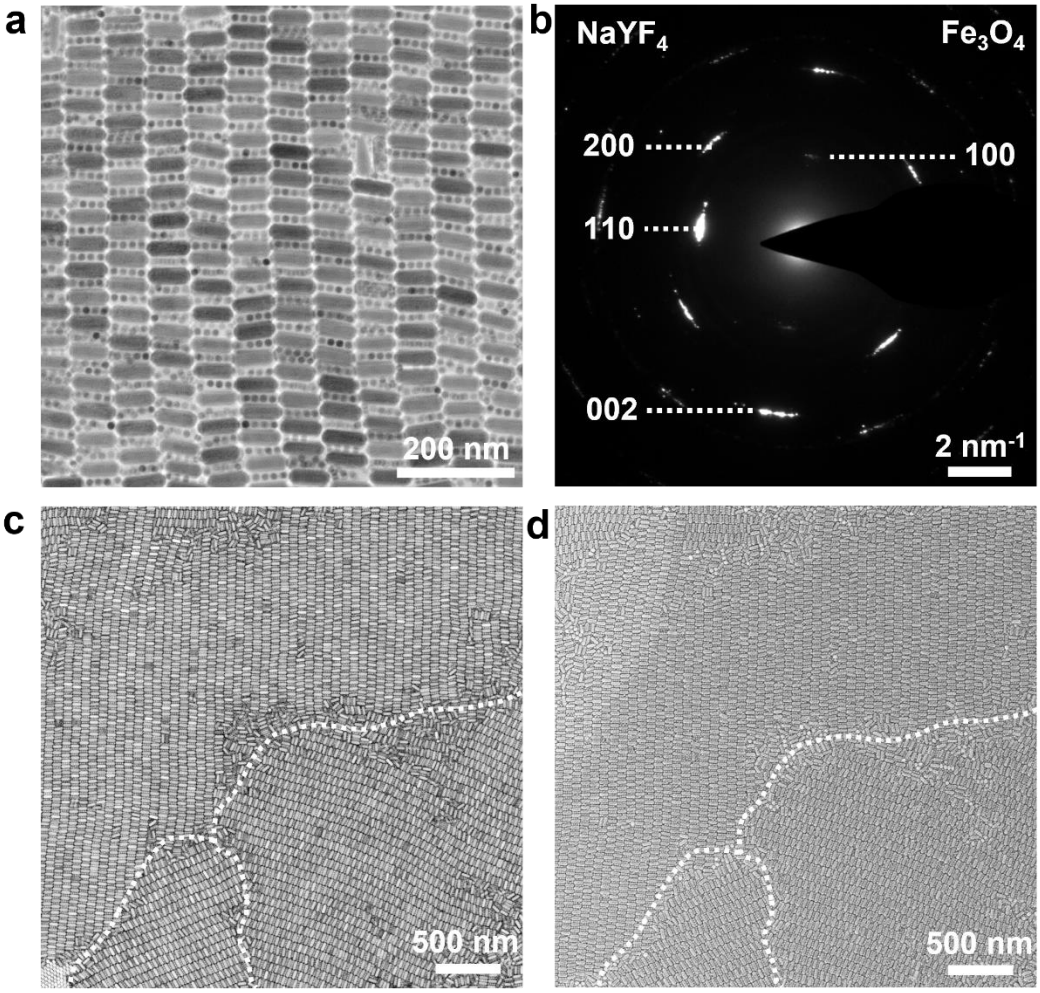

Figure S5. (a) Low-magnification HAADF-STEM image of Quasi-2D AB_2 BNSLs co-assembled from NR-2 and 13.1 nm Fe_3O_4 NSs; (b) WAED pattern; (c) low-magnification HAADF-STEM image showing three distinct domains; (d) Low-magnification SEM image.

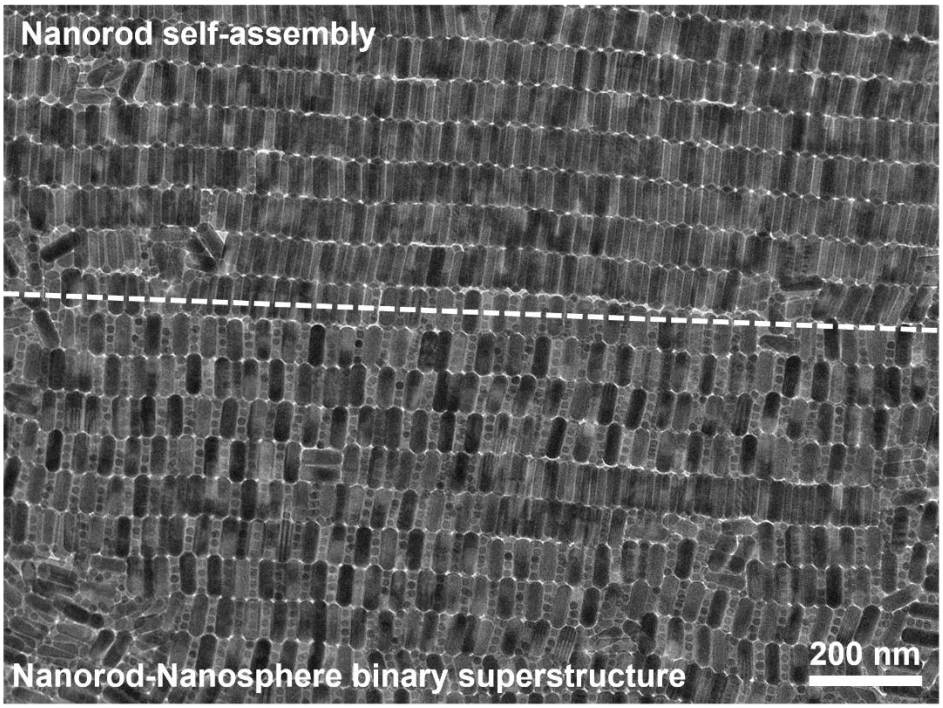

Figure S6. TEM image showing the coexistence of Quasi-2D AB_2 BNSLs formed from NR-2 and 13.1 nm Fe_3O_4 NSs and rod-only assemblies within the same sample.

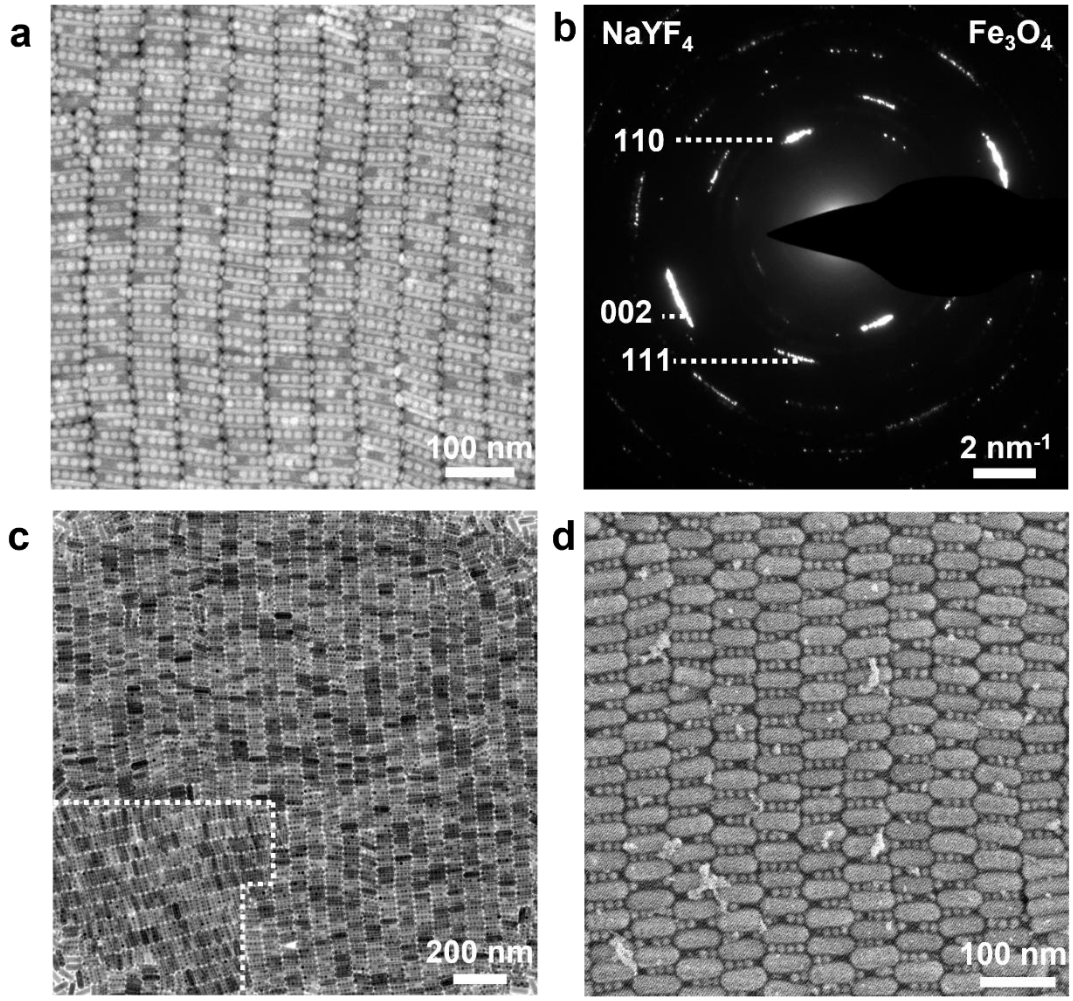

Figure S7. (a) Low-magnification HAADF-STEM image of Quasi-2D AB_4 BNSLs co-assembled from NR-2 and 13.1 nm Fe_3O_4 NSs; (b) WAED pattern; (c) low-magnification TEM image showing two distinct domains; (d) SEM image.

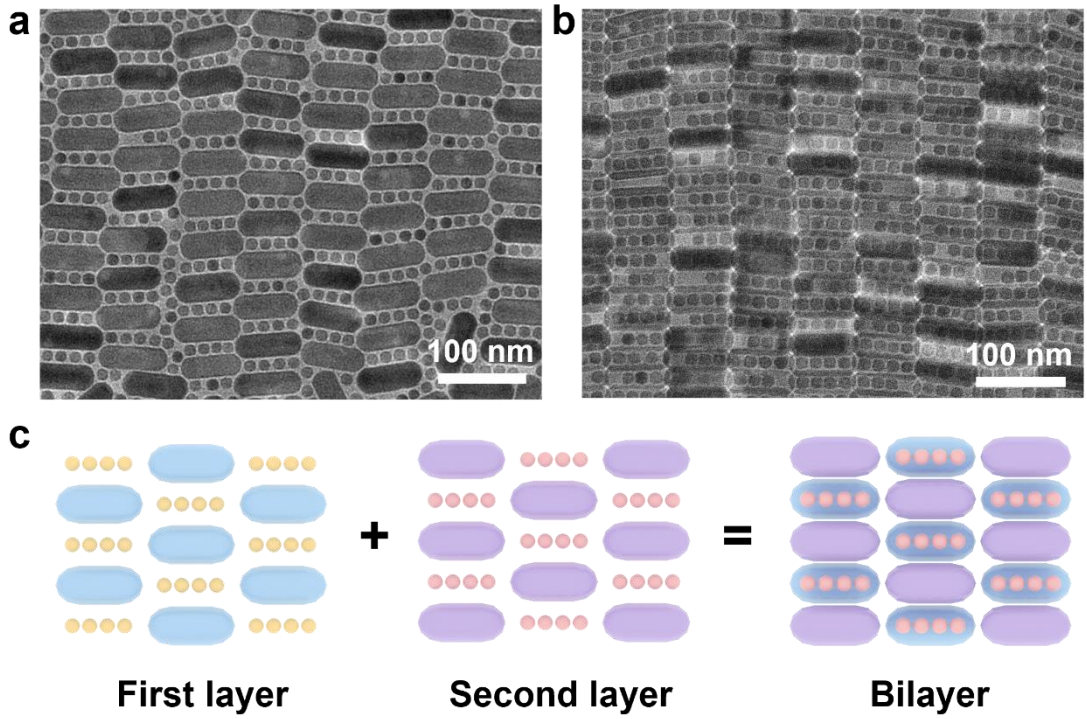

Figure S8. (a) TEM image of the first layer of Quasi-2D AB_4 BNSLs, showing an ordered structure where four NSs act as a single cluster unit and alternately pack with NRs; (b) TEM image of the bilayer structure; (c) corresponding schematic models of the first layer, second layer, and the bilayer configuration.

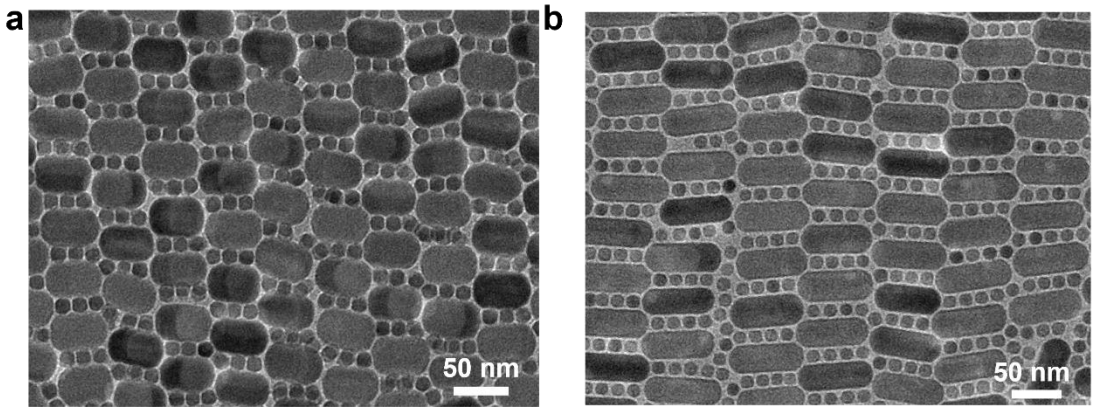

Figure S9. (a) TEM image of NR-1 (31.9 × 50.0 nm) assembled with 13.1 nm Fe_3O_4 NSs; (b) TEM image of NR-2 (26.4 × 71.8 nm) assembled with 13.1 nm Fe_3O_4 NSs. With increasing nanorod length, the cluster size of nanospheres coordinated with a single nanorod increases from three to four in projection, indicating a length-dependent modulation of rod–sphere packing configuration.

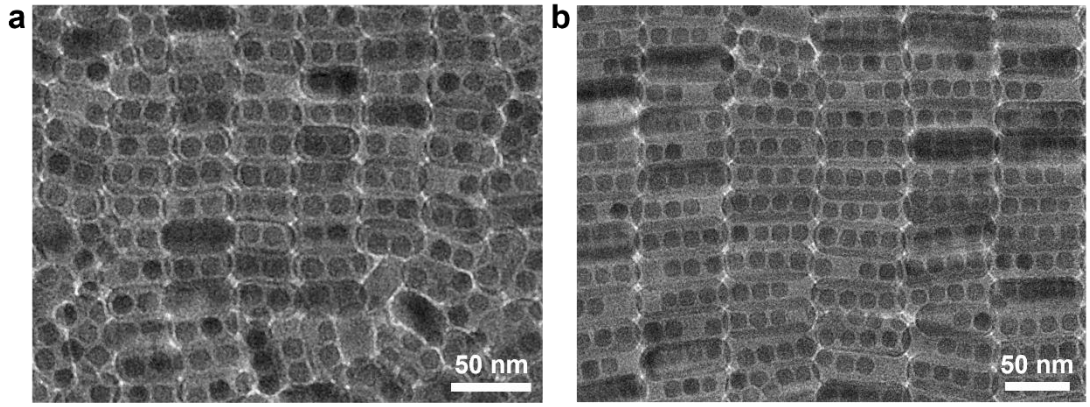

Figure S10. (a) TEM image showing the co-assembly of NR-3 (21.2 × 45.4 nm) and 13.1 nm Fe_3O_4 NSs, where each nanorod accommodates two nanospheres along its length; (b) TEM image showing the co-assembly of NR-2 (26.4 × 71.8 nm) and 13.1 nm Fe_3O_4 NSs, where each nanorod accommodates four nanospheres. At a fixed sphere size, the number of accommodated spheres increases with nanorod length.

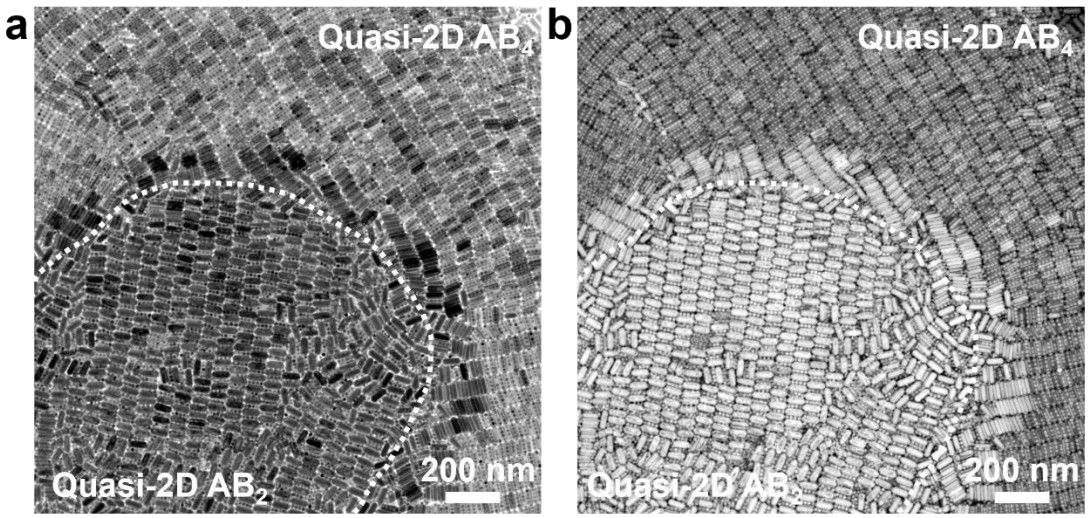

Figure S11. (a) TEM and (b) HAADF-STEM images of the coexisting phase of Quasi-2D AB_2 and AB_4 BNSLs.

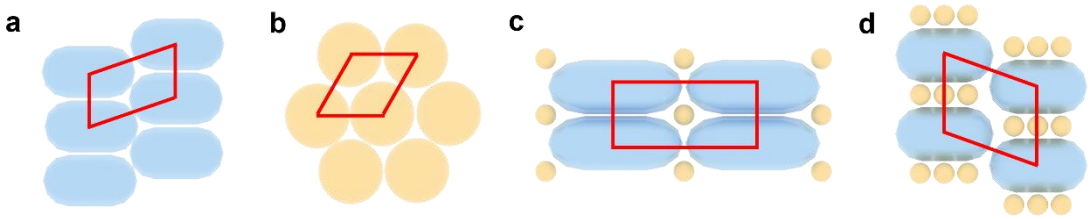

Figure S12. Schematics showing the geometric calculation of the packing efficiencies for (a) single-component NR assemblies, (b) single-component NS assemblies, (c) AB-*pmm* BNSLs, and (d) AB_6-*p*2 BNSLs. The red outlines indicate the corresponding unit cells used for the packing efficiency calculations.

The projected area of an individual NR is estimated as: $\boldsymbol{S_{Rod} = \frac{\pi {d_{Rod}}^2}{4} + \mathbf{d}(L - d_{Rod})}$

The projected area of an individual NS is calculated as: $\boldsymbol{S_{Sphere} = \frac{\pi {d_{Sphere}}^2}{4}}$

The packing density (η_{NR}) of single-component NR SLs is calculated by:

$$\boldsymbol{\eta_{NR} = \frac{S_{Rod}}{L \times d_{Rod}} = 92.25\%}$$

The packing density (η_{NS}) of single-component NS SLs is calculated by:

$$\boldsymbol{\eta_{NS} = \frac{\pi\left(\frac{d_{Sphere}}{2}\right)^2}{2\sqrt{3}\left(\frac{d_{Sphere}}{2}\right)^2} = 90.69\%}$$

For AB-*pmm* BNSLs, the packing density is given by:

$$\boldsymbol{\eta_{AB-pmm} = \frac{S_{Sphere}+S_{Rod}}{S_{Unit\ cell}} = \frac{S_{Sphere}+S_{Rod}}{d_{Rod} \times \left(L + \frac{d_{Sphere}}{2}\right)} = 91.11\%}$$

For AB_6-*p*2 BNSLs, the packing density is given by:

$$\boldsymbol{\eta_{AB_6-p2} = \frac{S_{Sphere}+3 \times S_{Rod}}{S_{Unit\ cell}} = \frac{S_{Sphere}+3S_{Rod}}{(d_{Rod}+d_{Sphere}) \times L} = 79.04\%}$$

The projected 2D packing efficiencies indicate that the AB-*pmm* BNSLs achieve packing densities comparable to those of close-packed single-component NR and NS assemblies, while the AB_6-*p*2 phase retains relatively high space-filling efficiency despite its more open binary arrangement. These results suggest that cooperative NR–NS packing enables efficient structural organization in the co-assembled superlattices.

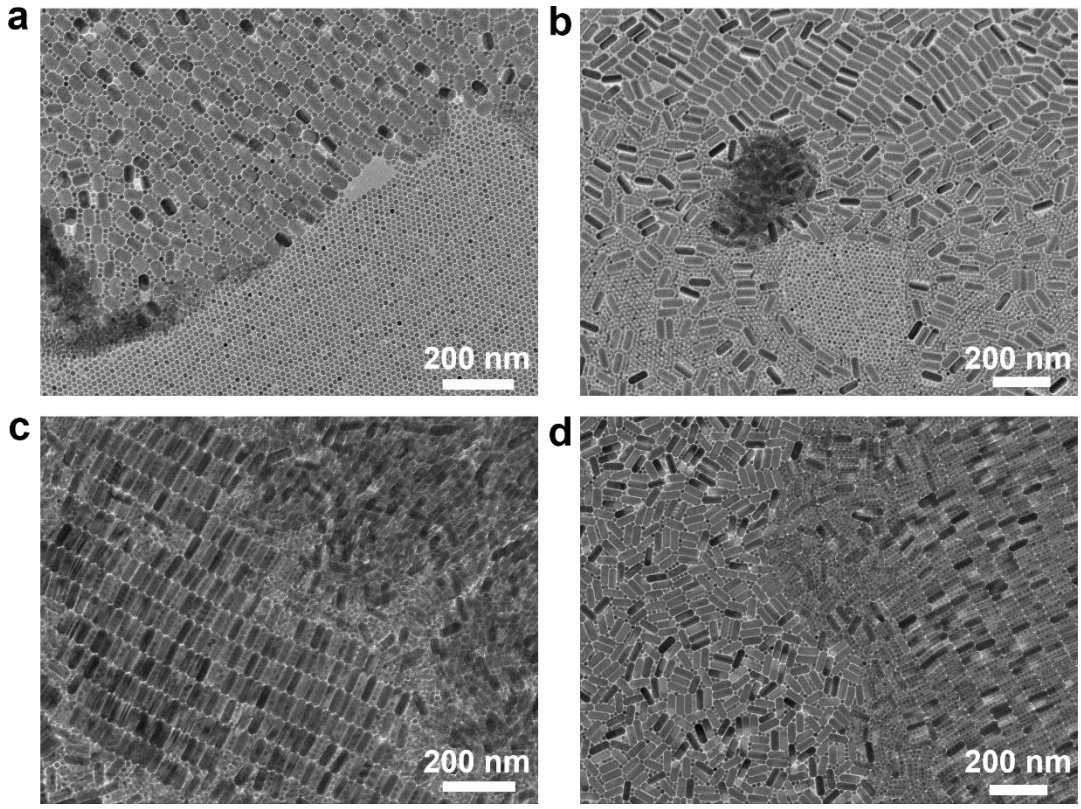

Figure S13. TEM images showing the coexistence of binary superlattices and single-component nanosphere phases: (a) AB-*pmm* BNSLs; (b) AB_6-*p*2 BNSLs; (c) Quasi-2D AB_2 BNSLs; and (d) Quasi-2D AB_4 BNSLs.

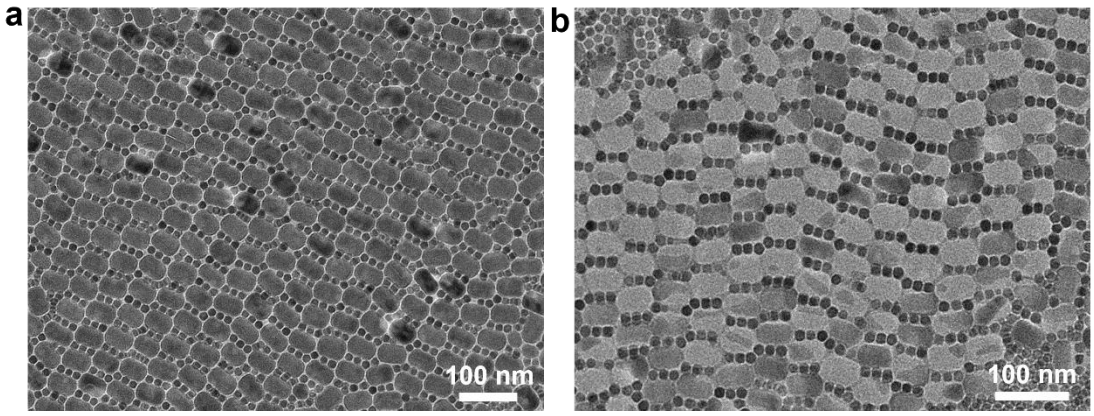

Figure S14. (a) TEM image of Pristine AB_6-*p*2 BNSLs; (b) nanosphere arrays obtained after selective etching of nanorods.

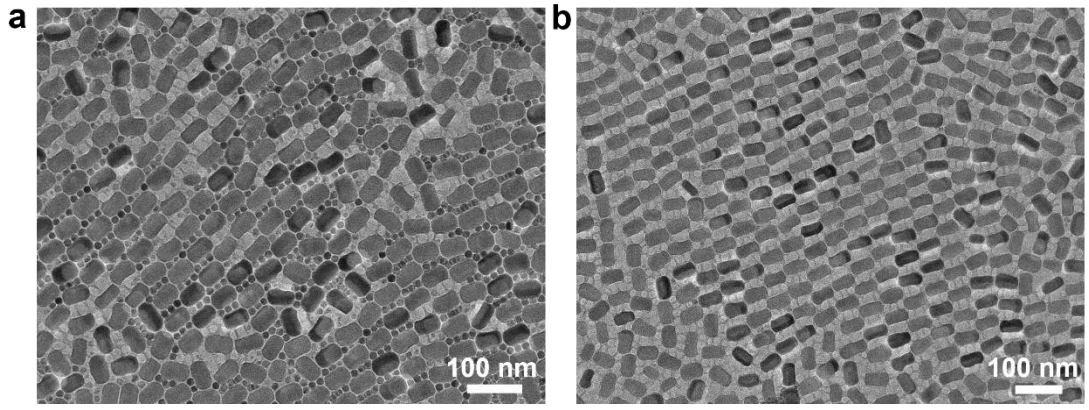

Figure S15. (a) TEM image showing the initial partial etching of nanospheres within the AB_6-*p*2 BNSLs. (b) TEM image of the ordered nanorod arrays obtained after the complete removal of the nanospheres.

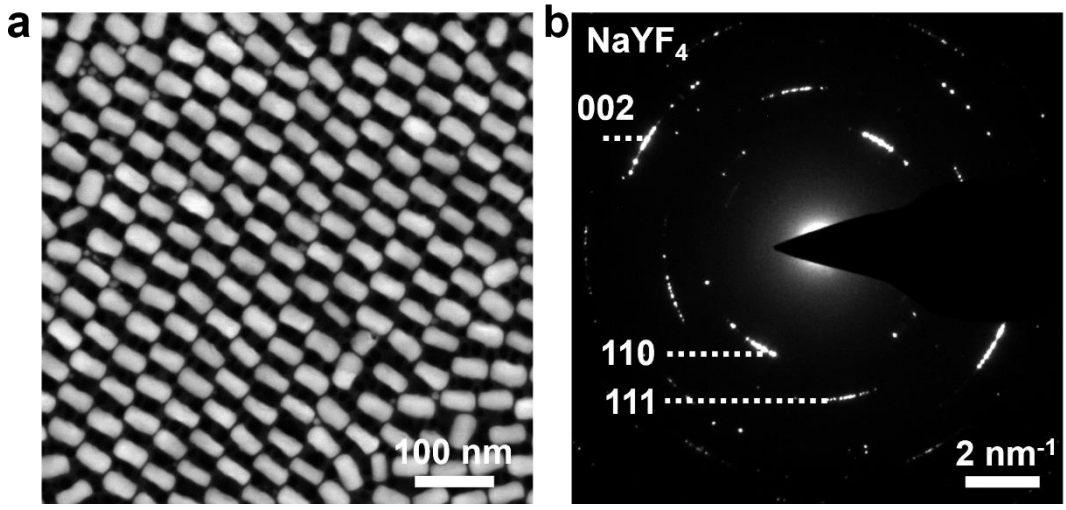

Figure S16. (a) HAADF-STEM image and (b) corresponding WAED pattern of the nanorod arrays derived from AB_6-*p*2 BNSLs via selective etching of nanospheres.

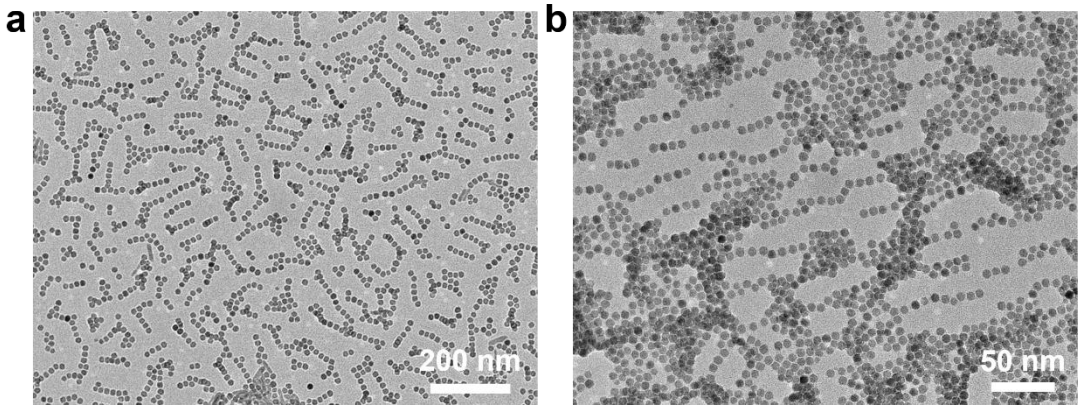

Figure S17. (a) TEM image of nanosphere assemblies obtained by etching nanorods from Quasi-2D AB_4 BNSLs. (b) Locally ordered four-sphere clusters lacking long-range order.

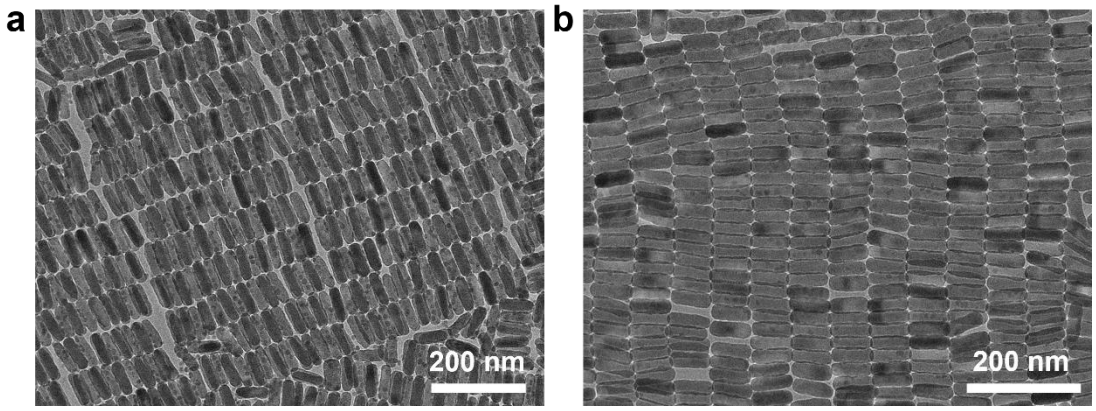

Figure S18. (a, b) TEM images illustrating the progressive etching of nanospheres from Quasi-2D AB_4 BNSLs, ranging from (a) initial partial etching to (b) complete removal to produce nanorod arrays.

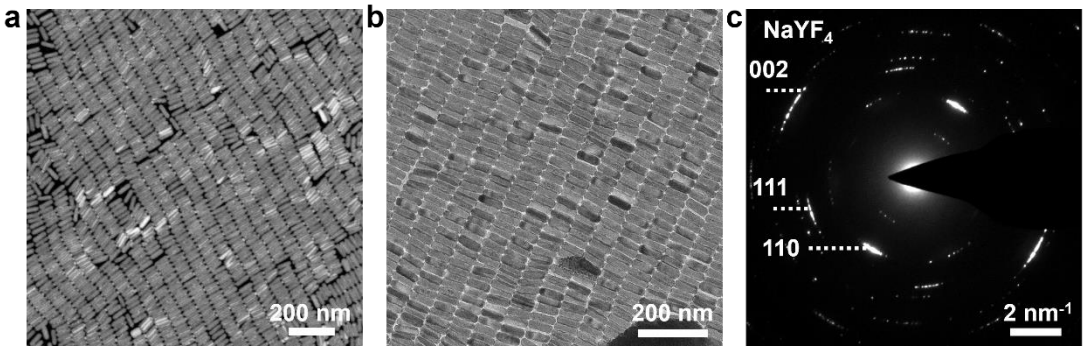

Figure S19. (a) Low-magnification HAADF-STEM image, (b) TEM image, and (c) corresponding WAED pattern of the nanorod arrays derived from Quasi-2D AB_4 BNSLs via selective etching of nanospheres.

Table S1. Summary of the assembly results of d_{Sphere}/d_{Rod} = 0.35 and 0.37.

d_{Sphere}/d_{Rod}	N_{Sphere}/N_{Rod}	Assembly results	Characterization
0.35	10.0	Phase separation	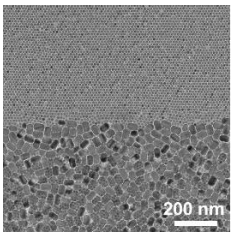
0.37	1.5	Disorder	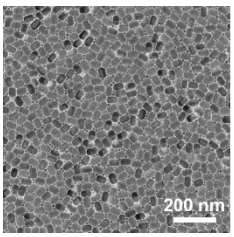
	4.0	Disorder	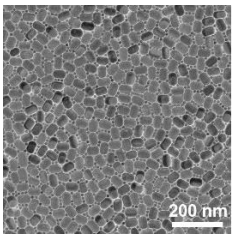
	8.0	Phase separation	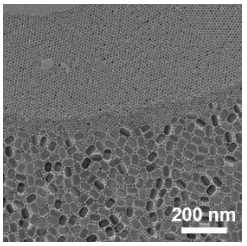
	10.0	Phase separation	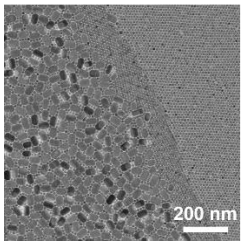
	12.0	Phase separation	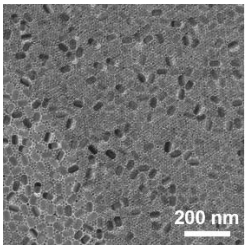

Table S2. Summary of the assembly results of d_{Sphere}/d_{Rod} = 0.40.

d_{Sphere}/d_{Rod}	N_{Sphere}/N_{Rod}	Assembly results	Characterization
0.40	8.8	AB_6-*p*2	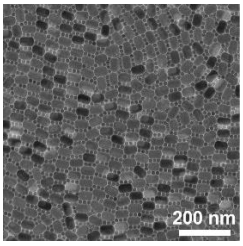
	9.1	AB_6-*p*2	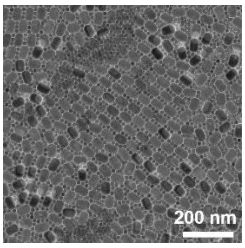
	9.7	AB_6-*p*2	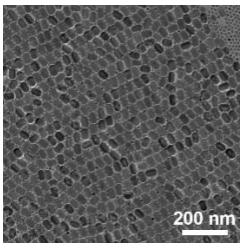
	10.0	Phase separation	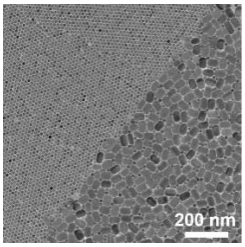
	11.1	Phase separation	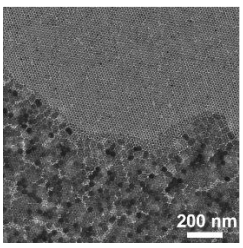
	12.0	Phase separation	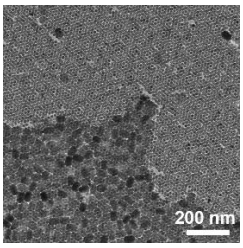

Table S3. Summary of the assembly results of d_{Sphere}/d_{Rod} = 0.49.

d_{Sphere}/d_{Rod}	N_{Sphere}/N_{Rod}	Assembly results	Characterization
0.49	2.0	Disorder	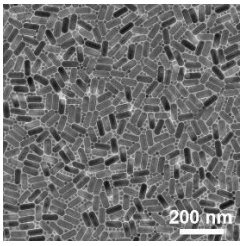
	3.0	Disorder	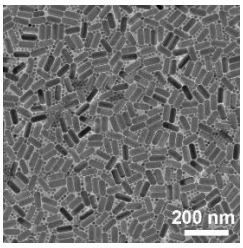
	3.3	AB-*p*mm	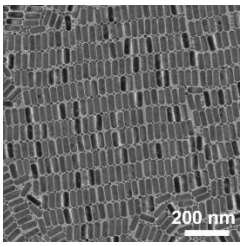
	3.9	AB-*p*mm	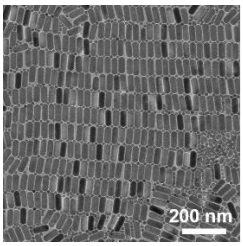
	4.4	Quasi-2D (I)	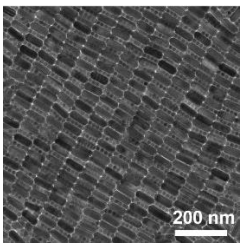
	4.7	Quasi-2D (I)	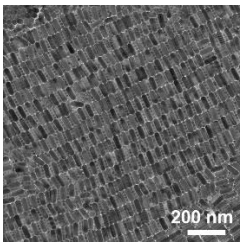

Table S4. Summary of the assembly results of d_{Sphere}/d_{Rod} = 0.49 and 0.52.

d_{Sphere}/d_{Rod}	N_{Sphere}/N_{Rod}	Assembly results	Characterization
0.49	5.1	Quasi-2D (I)	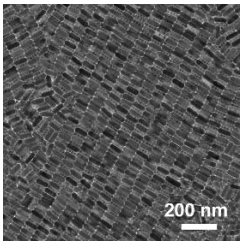
	5.5	Disorder	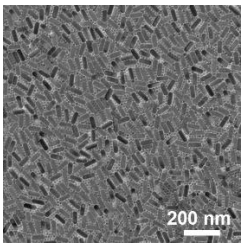
	6.0	Quasi-2D (II)	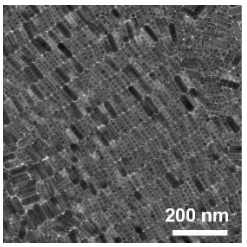
	6.6	Quasi-2D (II)	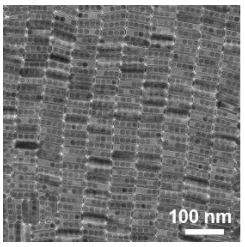
	7.8	Quasi-2D (II)	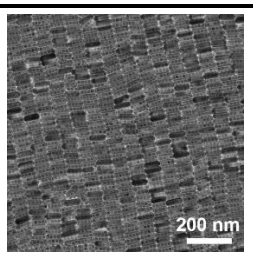
0.52	8.0	Disorder	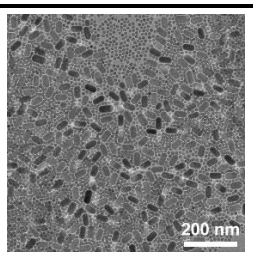

Table S5. Summary of the assembly results of d_{Sphere}/d_{Rod} = 0.54.

d_{Sphere}/d_{Rod}	N_{Sphere}/N_{Rod}	Assembly results	Characterization
0.54	0.2	Disorder	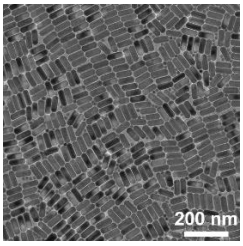
	0.5	Disorder	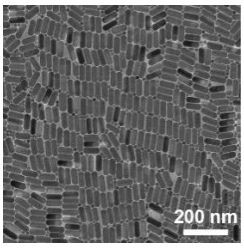
	1.0	Disorder	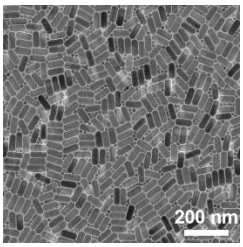
	3.0	Disorder	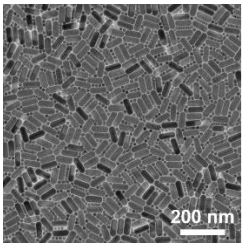
	4.0	Disorder	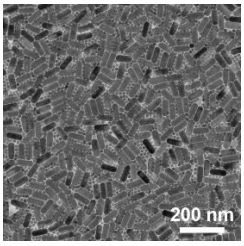
	10.0	Phase separation	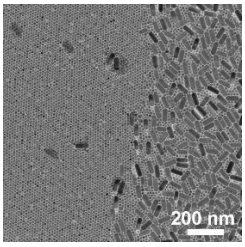

Table S6. Summary of the assembly results of d_{Sphere}/d_{Rod} = 0.61, 0.74 and 0.75.

d_{Sphere}/d_{Rod}	N_{Sphere}/N_{Rod}	Assembly results	Characterization
0.61	6.0	Disorder	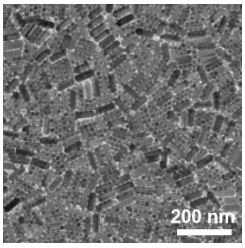
	8.0	Disorder	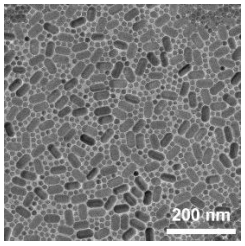
	10.0	Phase separation	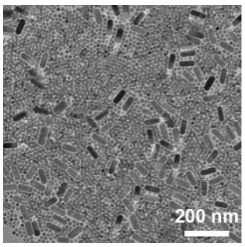
0.74	0.3	Disorder	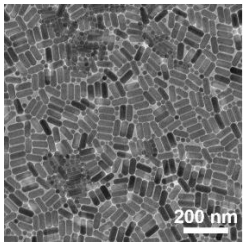
	0.4	Disorder	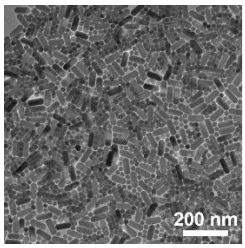
0.75	9.0	Phase separation	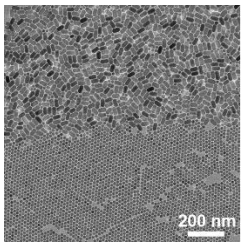

Table S7. Summary of the assembly results of d_{Sphere}/d_{Rod} = 0.80, 1.10 and 1.28.

d_{Sphere}/d_{Rod}	N_{Sphere}/N_{Rod}	Assembly results	Characterization
0.80	3.5	Disorder	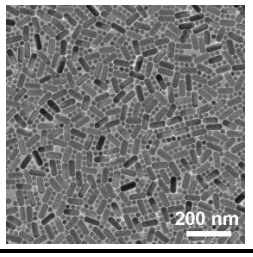
1.10	2.0	Disorder	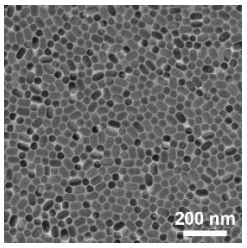
	4.0	Disorder	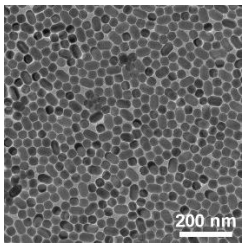
	8.0	Phase separation	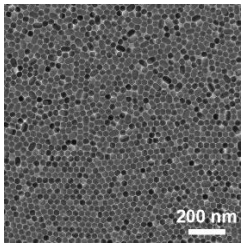
	10.0	Phase separation	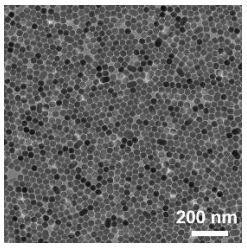
1.28	2.5	Disorder	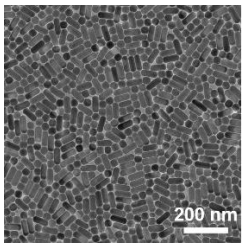

Table S8. Summary of the assembly results of d_{Sphere}/d_{Rod} = 1.28.

d_{Sphere}/d_{Rod}	N_{Sphere}/N_{Rod}	Assembly results	Characterization
1.28	6.0	Phase separation	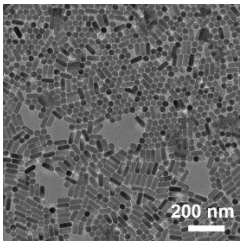

Reference

1. D. Liu, X. Xu, Y. Du, X. Qin, Y. Zhang, C. Ma, S. Wen, W. Ren, E. M. Goldys, J. A. Piper, S. Dou, X. Liu and D. Jin, *Nat. Commun.*, 2016, **7**, 10254.

2. J. Park, K. An, Y. Hwang, J. G. Park, H. J. Noh, J. Y. Kim, J. H. Park, N. M. Hwang and T. Hyeon, *Nat. Mater.*, 2004, **3**, 891–895.

3. A. Dong, J. Chen, P. M. Vora, J. M. Kikkawa and C. B. Murray, *Nature*, 2010, **466**, 474–477.

4. D. Lei, H. Wang, T. Wang, F. Wu, N. Ding, Y. Wang, T. Li and A. Dong, *Chem. Commun.*, 2026, **62**, 6596–6599.